

Post-print: *Nanoscale* , 2010, 2, 936-941

DOI: 10.1039/B9NR00338J

Environmentally responsive nanoparticle -based luminescent optical resonators

Olalla Sánchez-Sobrado , Mauricio E. Calvo , Nuria Núñez , Manuel Ocaña , Gabriel Lozano and Hernán Míguez *

Instituto de Ciencia de Materiales de Sevilla, Consejo Superior de Investigaciones Científicas-Universidad de Sevilla, Américo Vespucio 49, , 41092 Sevilla, Spain. E-mail: hernan@icmse.csic.es

In this work, we demonstrate that optical resonators built using all-nanoparticle -based porous building blocks provide a responsive multifunctional matrix, totally different emission spectra being attained from the same embedded luminescent nanophosphors under varying environmental conditions. We show a clear correlation between modifications in the ambient surroundings, the induced changes of the resonant modes, and the resulting variations in the emission response. The method is versatile and allows nanophosphors of arbitrary shape to be integrated in the cavity. By precise control of the spectral features of the optical resonances, luminescence is strongly modulated in selected and tuneable wavelength ranges. Applications in the fields of sensing and detection are foreseen for these materials.

1. Introduction

Luminescent nanoparticles ^{1,2} present a wide range of applications in several fields, such as light emitting diodes,³ sensing,⁴ or bio labelling ^{.5–7} The spectral position and the width of emission bands can be tailored to match any visible or near infrared ranges by varying the composition and the size of nanoparticles ^{.8} Actually, from the spectral point of view, the available emission patterns of nanoparticles range from the narrow, atom-like ones of rare earth-based nanophosphors^{9,10} to the white light emission of certain semiconductor quantum dots ^{.11}

One way to control the emission of luminescent nanomaterials is to integrate them in optical resonators whose modes coincide with a range of frequencies emitted by the material.¹² By doing so, it is possible, in principle, to mould the emission spectrum , amplifying or suppressing luminescence in the desired spectral ranges.¹³ However, resonators operating in the visible and near infrared regions present structural features of sizes in the order of few hundreds of nanometres. This has, in turn, restricted the size of particles to be included in such cavities and, consequently, the range of luminescent particles whose emission can be tuned. Thus, while there exist several reports on the modification of luminescence from semiconductor quantum dots (with sizes typically below 10 nm) incorporated in different types of photonic nanostructures ^{,14–16} hardly any examples can be found on the integration of other optically active nanoparticles of arbitrary shape and composition in such matrices. In particular,

although the optical properties of rare earth ions integrated in periodic structures have attracted a great deal of interest,^{17–20} as far as we know, there are only two precedents in which infiltration of rare earth-based particles (nanophosphors) is performed in the large cavities of a three-dimensional photonic crystal.^{21,22} In these experiments, significant modification of the luminescence lifetime was observed at photonic band gap frequencies.

Herein, we show that rare earth-based nanophosphors of complex shape and of size in the order of a hundred nanometres can be embedded in all-nanoparticle -based optical cavities built up in one dimensional (1D) photonic crystals. Optical quality is preserved due to the ability of the embedding nanoparticles to adapt to any arbitrary shape of the guest material. The photon modes of these cavities can be precisely controlled, allowing for precise tailoring of the photoluminescence of the nanophosphors. In particular, we demonstrate that their luminescence can be selectively amplified or suppressed in tuneable wavelength ranges along the direction perpendicular to the slabs. The porous character of the nanoparticle -based building blocks of these optical cavities provides a responsive multifunctional matrix. Liquid compounds can easily flow in and out of the structure, totally different emission spectra being attained from the same nanophosphors by the environmentally induced changes of the photonic modes of the cavity when immersed in different liquids. Furthermore, we show that the intensity of selected emission lines gradually varies in response to changes of partial pressure in the surrounding atmosphere, as a result of modifications of the optical resonance caused by adsorption and condensation of compounds from the gas phase within the pores .

2. Results and discussion

2.1 Structure of nanoparticle -based optical resonators

Fig. 1 pictures a model of the proposed hierarchical nanostructure . The optical resonator is formed by sandwiching a layer of rhombic Eu-doped nanophosphors between two multilayers made of alternate coatings of spherical SiO₂ particles and smaller TiO₂ nanocrystals of arbitrary shape. The structure of the optical cavity is shown in detail in the amplified scheme drawn on the right, in which its different parts can be readily identified. The thickness of each component layer in the structure can be precisely determined through the deposition conditions, which in turn allow control over its optical response.

Images of the actual intermediate and final structures are shown in Fig. 2, in which pictures attained using a field emission scanning electron microscope (FESEM , Hitachi 5200) are displayed. Fig. 2(a) and 2(b) show low and high magnification top views, respectively, of the surface of the silica nanoparticle layer deposited on top of the first photonic crystal, after the deposition of the rhombic lanthanide nanoparticles whose emission we seek to controllably modify. Their number density on such surface is uniform at the few microns length scale that is optically tested herein. Fig. 2(c) and 2(d) show cross sections of the final structure, i.e., after the second half of the optical cavity and the second Bragg mirror have been built up and thermally annealed. It is clear from these images that the total thickness of the optical cavity is primarily determined by the thickness of the SiO₂ nanoparticles surrounding the thin layer of Eu-doped nanoparticles . Also, they demonstrate that, due to the ability of the silica beads to form a uniform layer even onto relatively rough surfaces, the presence of the nanophosphors does not alter the structural, and hence optical, quality of the ensemble.

2.1 Optical properties

Photoluminescence and reflectance spectra were obtained using a LabRam spectrophotometer attached to a microscope operating in reflection mode with a 10× objective with 0.1 numerical aperture (light cone angle $\pm 5.7^\circ$). Emission was measured using the $\lambda = 532$ nm line of a diode pumped doubled-frequency Nd-YAG solid state laser as the excitation source. The laser beam impinged on the sample along the direction perpendicular to the layers and luminescence was collected with the same objective employed to illuminate the sample. Thus, only experimental evidence of emission intensity modulation effects along this particular direction will be presented here.

The photoluminescence spectrum of the nanophosphor layer employed as reference is shown in Fig. 3(a). The emission bands arising from the $5D_0 \rightarrow 7F_J$ transitions characteristic of Eu^{3+} can be clearly identified and are indicated in the figure.²³ Aiming at creating a photonic environment capable of controllably modifying this emission, each one of the multilayers surrounding the optical cavity is designed to behave as a dielectric mirror in a wide wavelength range that includes the spectral positions at which the nanophosphor emission takes place. Inclusion of a middle SiO_2 layer, into which the nanophosphors have been integrated, as shown in Fig. 1 and 2, breaks the translational symmetry of the lattice and gives rise to a resonant mode, characteristic of an optical cavity. Such a mode is an allowed state in the forbidden photonic band gap, and can then be readily identified as a dip in the reflectance spectrum of the structure. These can be seen in the reflectance spectra shown in Fig. 3(b) and 3(c) (thin black lines), taken from samples in which the nanoparticle Bragg mirrors used to surround the optical cavity are three and five unit cells thick, respectively. In both examples, the thickness of the middle SiO_2 layer was chosen so that the resonance matches the nanophosphor emission line observed at $\lambda = 708$ nm, corresponding to the $5D_0 \rightarrow 7F_4$ transition. The corresponding photoluminescence spectra measured from the layer of sandwiched nanophosphors is plotted in Fig. 3(b) and 3(c) as thick red lines. The most intense emission peaks at $\lambda = 610$ nm and $\lambda = 628$ nm, resulting from the transitions $5D_0 \rightarrow 7F_2$, are first partially, Fig. 3(b), and then dramatically, Fig. 3(c), reduced, while the originally secondary luminescence maximum at $\lambda = 708$ nm is gradually amplified as we increase the thickness of the Bragg mirrors, first twice and then five times, when three and five unit cell Bragg mirrors are used, respectively.

The enhancement caused by a microcavity on the luminescence intensity of embedded active species emitting in resonance with the cavity mode is a well-known effect that has been thoroughly described before.²⁴ It can be related to the quality factor Q ,²⁵ defined as the quotient between the spectral position and the width of the resonant mode, $\omega_R/\Delta\omega_R$. The value of Q is largely determined by the reflectance of the periodic structure surrounding the cavity, which depends on the refractive index contrast existing between the layers ($n_{\text{TiO}_2}/n_{\text{SiO}_2} = 1.69/1.24 = 1.36$), the filling fraction ($ff_{\text{SiO}_2} = 55\%$, $ff_{\text{TiO}_2} = 45\%$), and on the number of unit cells present in the mirrors. Refractive index and filling factor values are extracted from the fitting of the measured reflectance spectra. Experimental Q factors can be estimated from the position and full width at half maximum of the dip associated to the resonance detected in the reflectance spectra of Fig. 3(b) and 3(c). From these data, we estimate that the optical resonators built using three unit cell Bragg mirrors present $Q \approx 8$,

while for those that incorporate five unit cell mirrors $Q \approx 30$, in good qualitative, although not quantitative, agreement with the trend observed for the luminescent emission intensity enhancement factor at $\lambda = 708$ nm. A rigorous theoretical description of the effect²⁶ and more experimental work are needed in order to confirm if the mechanism of enhancement is related to the modification of the radiative decay channels, as has been observed before.²⁷ For the purposes pursued herein, that is, the demonstration of the strong effect of the porous resonator on the luminescence of embedded particles and, most importantly, its environmental dependence, the results shown in Fig. 3 and 4 are proof enough.

2.3 Response to environmental changes

The porous nature of the multilayer renders the photonic structure responsive to variations in the environment. It has recently been proven that a gradual increase of the ambient vapor pressure gives rise to condensation within the mesopores, thus changing the refractive index of the layers, and consequently the reflectance of the Bragg stacks.²⁸ Also, these structures present a different color depending on the refractive index of the liquid they are soaked in.¹⁸ This same type of multilayers has also been shown to serve as matrices for organic dyes whose luminescence can be tailored by matching the photonic band gap edge to the emission band.²⁹ It should be noted that, as opposed to other standard luminescent species, such as organic dyes or quantum dots, the rare earth-based nanophosphors used in this work do not change their emission properties as a result of their interaction with fluids or gases, since the active ions are embedded in a protective yttrium fluoride matrix. This feature is particularly important to prevent unwanted variations of the luminescence that are not related to structural changes, which are the subject of our study. Another advantage of these nanophosphors is found in their ease of processing. As proven herein, these nanocrystals do not lose their luminescent properties when heated up to 450 °C, which is needed to mechanically stabilize the optical resonators that embed them. Neither organic dyes nor quantum dots can be heated up to such temperatures without being removed or degraded. These are actually the two main reasons supporting the use of nanophosphors to build optically active, environmentally responsive, optical resonators.

In the case of the optical cavities analyzed herein, the luminescence spectrum of the nanophosphors is finely modulated by the optical response of the photonic structure. Hence, infiltration of its void volume with a liquid should cause an abrupt and strong modification of the photoluminescence. This concept was proven by measuring the luminescence before and after infiltrating the lattice with a series of liquids of different refractive index, namely, methanol ($n = 1.33$), isopropanol ($n = 1.38$) and tetrahydrofuran ($n = 1.41$). Results are shown in Fig. 4. The red-shift of the cavity mode to $\lambda = 762$ nm, as seen in the reflectance spectrum of the soaked sample, causes the emission peak at $\lambda = 708$ nm to be off-resonance, its intensity being reduced by a factor of 10–2 with respect to that measured from the dry structure. At the same time, the shift of the photonic band gap edges now allows the propagation and detection of the fine bands at $\lambda = 610$ nm and $\lambda = 628$ nm. Please note that the ratio of intensities of such bands is rather different to that measured from the reference sample (see Fig. 4(a)). This ratio is also dependent on the refractive index of the guest liquid (see Fig. 4(b), (c), and (d)). These effects, although much less significant than for the resonant frequencies of the cavity, are a consequence of the enhancement and suppression of the photoluminescence that occurs at

wavelengths close to the photonic band gap edge. In Fig. 5 we plot the variation of the position of the resonant mode (λ_R , black solid circles) and the higher energy edge of the Bragg peak (λ_{HE} , red open circles) as we increase the refractive index of the embedded liquid. In both cases, linear behavior is observed, which is in good agreement with theoretical predictions. The spectral position of the emission lines of the embedded nanophosphors are also drawn as dashed horizontal lines.

In order to further prove the sensitivity and selectivity of the optical response to changes in the ambient surroundings, we analyzed the changes induced in both the position of the resonant mode and the luminescence of the embedded nanophosphors by gradual variations of the partial vapor pressure of different compounds. In order to do so, the multilayer structures were introduced in a closed chamber in which the partial pressure of a volatile liquid could be varied from $P/P_0 = 0$ to 1 (P_0 being the saturation vapour pressure of the liquid at room temperature). The chamber possesses a flat quartz window through which the reflectance spectra at normal incidence and the luminescence spectra could be measured in situ. In Fig. 6, a series of reflectance (thin solid lines) and luminescence (thick solid lines) spectra attained at different values of P/P_0 of isopropanol vapor in the chamber are plotted. It can be clearly seen that the intensity of the emission peak at $\lambda = 708$ nm slowly diminishes as the match with the resonant mode decreases due to its gradual red shift. This is a result of the increase of the average refractive index of the multilayer originating in the adsorption and later condensation of isopropanol onto the pore walls. Similar experiments were performed vaporizing toluene in the chamber. By plotting the evolution of the luminescence peak intensity versus P/P_0 one can obtain an adsorption isotherm whose particular features depend mainly on the refractive index of the adsorbed species. Two such curves obtained by vaporizing isopropanol ($n = 1.38$, black solid circles) and toluene ($n = 1.50$, red open circles) in the chamber are plotted in Fig. 7. It can be seen that, as expected, for a fixed P/P_0 , the adsorption of a higher refractive index liquid gives rise to larger shifts of the position of the resonant mode, and thus, to more abrupt drops of the emission peak intensity.

These results prove the sensitivity of the luminescence spectra of the embedded nanophosphors to the degree of matching between the resonant or forbidden modes and the emission lines. Furthermore, the variations observed depend, in a first approximation, on the refractive index of the guest compound, which implies selectivity of the response. This analysis shows the potential these structures may offer in the field of sensing and detection.

3. Experimental

The luminescent resonators presented herein were built by creating optical “defects” of controlled width within nanoparticle based Bragg reflectors. A layer of highly uniform red emitting Eu-doped yttrium fluoride (YF₃) nanophosphors was embedded in this defect layer in order to render it optically active. Such luminescent particles were chosen due to their higher thermal and chemical stability, which is provided by the YF₃ matrix, as well as for their low toxicity for the environment. The advantage of using nanophosphors over other types of luminescent nanomaterials or compounds for the purpose pursued herein was discussed in the previous section.

Nanophosphors suspended in ethylene glycol were obtained following an ionic liquid base recipe thoroughly described elsewhere.³⁰ Chemicals used were yttrium(III) acetate ($\text{Y}(\text{CH}_3\text{COO})_3 \cdot \text{XH}_2\text{O}$, Aldrich, 99.9%) and europium(III) nitrate ($\text{Eu}(\text{NO}_3)_3 \cdot 5\text{H}_2\text{O}$, Aldrich, 99.9%), which were selected as lanthanide precursors. 1-Butyl-2-methylimidazolium tetrafluoroborate, ($\text{C}_8\text{H}_{15}\text{BF}_4\text{N}_2$, [BMIM] BF_4 , Fluka, >97%) was used as fluoride source, and ethylene glycol (Fluka, <99.5%) as the solvent. All chemicals were used as received. The standard procedure for the synthesis of the rare earth fluoride nanoparticles was as follows. Weighted amounts of the rare earth precursors were dissolved in ethylene glycol under magnetic stirring, heating the vial at [similar]100 °C to facilitate the dissolution process, to get a 0.02 mol dm⁻³ solution of $\text{Y}(\text{OAc})_3$ and 0.002 mol dm⁻³ of $\text{Eu}(\text{NO}_3)_3$. The ethylene glycol solutions were cooled down to room temperature, after which the required volume of [BMIM] BF_4 to achieve a concentration 2.7 mol dm⁻³ of the ionic liquid was admixed, keeping the magnetic stirring. The final solutions (total volume = 5 cm³) were then aged for 15 h in tightly closed test tubes using an oven preheated at 120 °C. After aging, the resulting dispersions were cooled down to room temperature, centrifuged to remove the supernatants and washed, twice with ethanol and once with double distilled water. The resulting Eu-doped YF_3 particles present a flat (thickness 26 ± 1 nm) rhombic shape, whose long and short axes present lengths of 110 ± 10 nm and 38 ± 3 nm, respectively. A full electron microscopy and XRD characterization can be found in ref. 17.

The Bragg reflector porous multilayers were prepared by alternated deposition of TiO_2 and SiO_2 nanoparticulated suspensions, following a generic procedure based on spin-coating previously reported by our group.³¹ The unit cell repeated along the lattice is a bilayer of TiO_2 and SiO_2 nanoparticles. TiO_2 nanoparticulated sols were synthesized using a procedure based on the hydrolysis of titanium tetraisopropoxide ($\text{Ti}(\text{OCH}_2\text{CH}_2\text{CH}_3)_4$, 97% Aldrich, abbrev. TTIP) as it has been described before.³² TTIP was added to Milli-Q water. The white precipitate was filtered and washed several times with distilled water. The resultant solid was peptized in an oven at 120 °C for 3 h with tetramethylammonium hydroxide (Fluka). Finally, the suspension obtained was centrifuged at 14000 rpm for 10 min. SiO_2 nanocolloids were purchased from Dupont (LUDOX TMA, Aldrich). Both suspensions were diluted in methanol to 5% wt. and 3.5% wt. for TiO_2 and SiO_2 particles, respectively. These sols were deposited over zero fluorescence glass (Proscitech) using a spin coater (Laurell WS-400E-6NPP) in which both the acceleration ramp and the final rotation speed could be precisely determined. The first layer was deposited using 250 μL of SiO_2 sol, and the substrate was tilted and rotated to let the suspension cover the total glass surface. Then, the sample was accelerated at 5850 rpm s⁻¹ up to a final speed of 4000 rpm. The total spin-coating process (ramping-up and final speed) is completed in 60 s. Afterwards, the coated sample is maintained at 25 °C for five minutes in a closed chamber. Sequentially, another layer of a different type of nanoparticle is deposited following the procedure described above. The process is repeated until the desired number of unit cells has been deposited. The Bragg mirrors built for the study presented herein were made of alternate layers of SiO_2 and TiO_2 of thickness 110 and 75 nm, respectively.

In order to build the optical cavity, a layer of spherical SiO_2 nanoparticles of controlled thickness is deposited onto the already formed photonic crystal, which has been previously annealed at 450 °C to provide it with mechanical stability. Then, a nanophosphor layer is deposited onto such coating also using spin-coating. In this case, the precursor suspension is a

dispersion of 1.5% wt. of the previously described Eu-doped YF₃ nanoparticles in ethylene glycol, which is used to ensure the homogeneity of the deposited film. After this, another layer of SiO₂ nanoparticles of thickness similar to the one onto which the lanthanide nanoparticles have been deposited is spun. By doing so, the necessary rupture of the translational symmetry required to create an optical cavity is achieved. Finally, a second photonic crystal is deposited and annealed, so that the final structure presents mirror symmetry with respect to the Eu-doped YF₃ nanoparticle plane.

In order to quantify the magnitude of the modifications of the photoluminescence properties caused by the photonic structure, a reference sample was prepared consisting of just a layer of nanophosphors sandwiched between two SiO₂ nanoparticle layers, i.e., the exact same replica of the intermediate layer that behaves as an optical cavity when surrounded by the Bragg mirrors. All structures, reference and optical resonators, were annealed at 450 °C to provide them with mechanical stability, which allows the flow of liquids or gases through them without altering the architecture of the host .

4. Conclusions

We have proven a versatile method to build all-nanoparticle -based optical resonators that are able to integrate nanophosphors of arbitrary shape and sizes on the order of a hundred nanometres while maintaining their structural quality. These photonic structures allow for a precise tailoring of the light emission of nanomaterials embedded within by means of the control over the spectral dependence of the density of photon states. They constitute environmentally responsive matrices whose optical parameters can be controllably varied by condensation or infiltration of an external agent, which in turn causes strong changes in the photoluminescence. We foresee this effect could be advantageously put into practice for the development of novel sensing devices.

Acknowledgements

We thank the Spanish Ministry of Science and Innovation for funding provided under grants MAT2008-02166 and CONSOLIDER HOPE CSD2007-00007, as well as Junta de Andalucía for grant FQM3579. MEC, NN, and GL thank the Spanish Research Council for funding of their scholarships and contracts under the JAE program.

References

1. C. B. Murray, D. J. Norris and M. G. Bawendi, *J. Am. Chem. Soc.*, 1993, 115, 8706
2. A. P. Alivisatos, *Science*, 1996, 271, 933
3. V. L. Colvin, M. C. Schlamp and A. P. Alivisatos, *Nature*, 1994, 370, 354
4. I. L. Medintz, H. T. Uyeda, E. R. Goldman and H. Mattoussi, *Nat. Mater.*, 2005, 4, 435
5. J. K. Jaiswal, H. Mattoussi, J. M. Mauro and S. M. Simon, *Nat. Biotechnol.*, 2003, 21, 47
6. X. H. Gao, W. C. W. Chan and S. M. Nie, *J. Biomed. Opt.*, 2002, 7, 532
7. X. F. Yu, L. D. Chen, M. Li, M. Y. Xie, L. Zhou, Y. Li and Q. Q. Wang, *Adv. Mater.*, 2008, 20, 4118
8. X. Peng, L. Manna, W. Yang, J. Wickham, E. Scher, A. Kadavanich and A. P. Alivisatos, *Nature*, 2000, 404, 59
9. J. C. Boyer, L. A. Cuccia and J. A. Capobianco, *Nano Lett.*, 2007, 7, 847
10. J. W. Stouwdam and F. C. J. M. van Veggel, *Nano Lett.*, 2002, 2, 733
11. M. J. Bowers, J. R. McBride and S. J. Rosenthal, *J. Am. Chem. Soc.*, 2005, 127, 15378
12. K. J. Vahala, *Nature*, 2003, 424, 839
13. M. Bayer, T. L. Reinecke, F. Weidner, A. Larionov, A. McDonald and A. Forchel, *Phys. Rev. Lett.*, 2001, 86, 3168
14. J. P. Reithmaier, G. Sekl, A. Löffler, C. Hofmann, S. Kuhn, S. Reitzenstein, L. V. Keldysh, V. D. Kulakovskii, T. L. Reinecke and A. Forchel, *Nature*, 2004, 432, 197
15. P. Lodahl, A. F. van Driel, I. S. Nikolaev, A. Irman, K. Overgaag, D. Vanmaekelbergh and W. L. Vos, *Nature*, 2004, 430, 654
16. J. Li, B. Jia, G. Zhou, C. Bullen, J. Serbin and M. Gu, *Adv. Mater.*, 2007, 19, 3276
17. S. G. Romanov, A. V. Fokin and R. M. de la Rue, *Appl. Phys. Lett.*, 2000, 76, 1656
18. M. Li, P. Zhang, J. Li, J. Zhou, A. Sinitskii, V. Abramova, S. O. Klimonsky and Y. D. Tretyakov, *Appl. Phys. B: Lasers Opt.*, 2007, 89, 251
19. A. Ródenas, G. Zhou, D. Jaque and M. Gu, *Adv. Mater.*, 2009, 21, 3526
20. M. M. Lezhnina, F. Laeri and U. Kynast, *J. Lumin.*, 2009, 129, 1464
21. M. Aleshyna, S. Sivakumar, M. Venkataramanan, A. G. Brolo and F. C. J. M. van Veggel, *J. Phys. Chem. C*, 2007, 111, 4047
22. Z. X. Li, L. L. Li, H. P. Zhou, Q. Yuan, C. Chen, L. D. Sun and C. H. Yan, *Chem. Commun.*, 2009, 6616

23. E. W. J. L. Oomen and A. M. A. van Dongen, *J. Non-Cryst. Solids*, 1989, 111, 205
24. A. M. Vredenberg, N. E. J. Hunt, E. F. Schubert, D. C. Jacobson, J. M. Poate and G. J. Zydik, *Phys. Rev. Lett.*, 1993, 71, 517
25. X. P. Feng, *Opt. Commun.*, 1991, 83, 162
26. M. Wubs and A. Lagendijk, *Phys. Rev. E: Stat., Nonlinear, Soft Matter Phys.*, 2002, 65, 046612
27. J. M. Gérard, B. Sermage, B. Gayral, B. Legrand, E. Costard and V. Thierry-Mieg, *Phys. Rev. Lett.*, 1998, 81, 1110
28. S. Colodrero, M. Ocaña, A. R. González-Elipe and H. Míguez, *Langmuir*, 2008, 24, 9135
29. F. Scotognella, D. P. Puzzo, A. Monguzzi, D. S. Wiersma, D. Maschke, R. Tubino and G. A. Ozin, *Small*, 2009, 5, 2048
30. N. O. Nuñez and M. Ocaña, *Nanotechnology*, 2007, 18, 455606
31. S. Colodrero, M. Ocaña and H. Míguez, *Langmuir*, 2008, 24, 4430
32. S. D. Burnside, V. Shklover, C. Barbé, P. Comte, F. Arendse, K. Brooks and M. Grätzel, *Chem. Mater.*, 1998, 10, 2419

Figure captions

Figure 1. Model of the proposed all-nanoparticle -based optical resonator. Spherical beads represent SiO₂ nanocolloids, smaller ones of irregular shape are TiO₂ nanocrystals and (red) rhombic particles are the embedded nanophosphors. On the right, the different components of the optical cavity are amplified and separated for the sake of clarity.

Figure 2. FESEM images showing a (a) low and (b) high magnification top views of a layer of rhombic shape europium-doped nanophosphors deposited onto a SiO₂ and TiO₂ nanoparticle multilayer. Spherical particles are SiO₂ nanocolloids. The picture displayed in (c) shows the cross section of a periodic multilayer made of 20 alternated layers (10 unit cells) made of SiO₂ and TiO₂ nanoparticles containing an optical cavity in the middle. The structure of the optical cavity, made of two silica layers sandwiching the nanophosphors, is shown in detail in (d).

Figure 3. (a) Luminescence spectrum obtained from the reference sample, consisting of a nanophosphor layer sandwiched between two SiO₂ layers deposited on zero-fluorescence glass. The corresponding electronic transitions in Eu³⁺ are indicated. Luminescence (thick red line) and reflectance (thin black line) spectra obtained from nanophosphor-containing optical resonators built using Bragg mirrors made of (b) three and (c) five unit cells .

Figure 4. Luminescence (thick lines) and reflectance (thin lines) spectra obtained from a nanophosphor -containing optical resonator built using two Bragg mirrors made of 5 unit cells (a) before and after being infiltrated with (b) methanol, (c) isopropanol, and (d) tetrahydrofuran.

Figure 5. Variation of the spectral position of the resonant mode, λ_R , (black solid circles) and the higher energy edge of the Bragg peak, λ_{HE} , (red open circles) with the refractive index of the infiltrated liquid. Data were attained from the curves shown in Fig. 4 plus similar ones obtained for ethanol ($n = 1.37$). Horizontal dashed lines indicate the spectral position of the three main emission lines of the nanophosphors. Lines connecting data points are just a guide for the eye.

Figure 6. Luminescence (thick lines) and reflectance (thin lines) spectra obtained from a nanophosphor -containing optical resonator built using two Bragg mirrors made of 5 unit cells after being exposed to a gradually increasing partial pressure of isopropanol vapor, namely (a) $P/P_0 = 0$ (b) $P/P_0 = 0.07$, (c) $P/P_0 = 0.19$, (d) $P/P_0 = 0.66$, and (e) $P/P_0 = 1$.

Figure 7. Variation of the photoluminescence intensity of the emission line located at $\lambda = 708$ nm as the partial pressure of isopropanol (black solid circles) and toluene (red open circles) increases in the chamber.

Figure 1

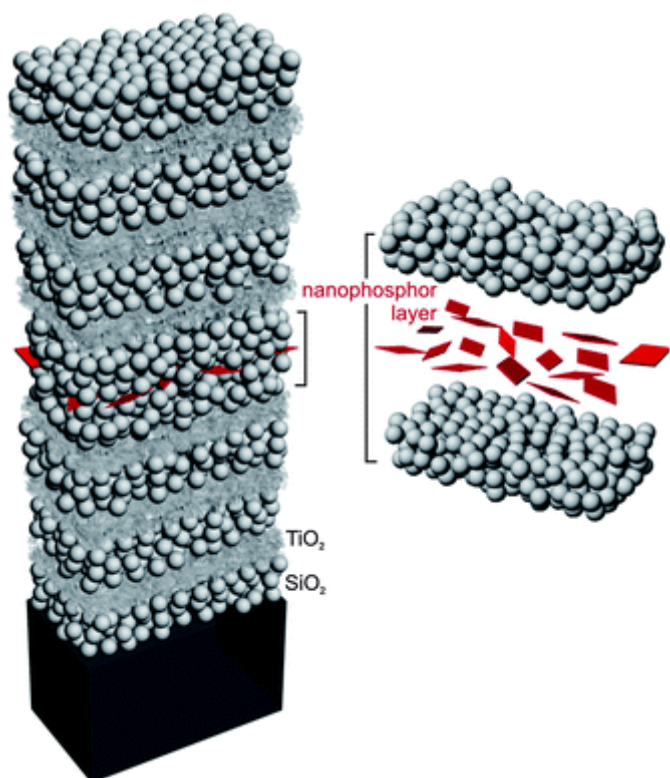


Figure 2

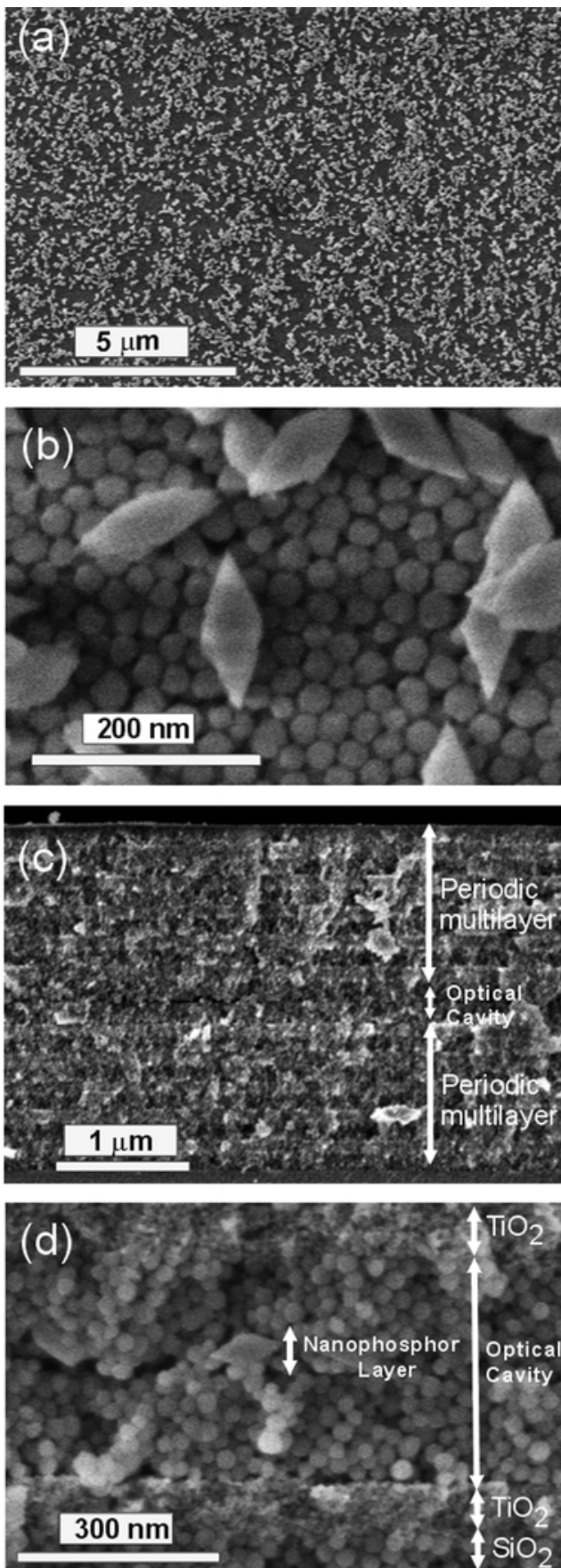


Figure 3

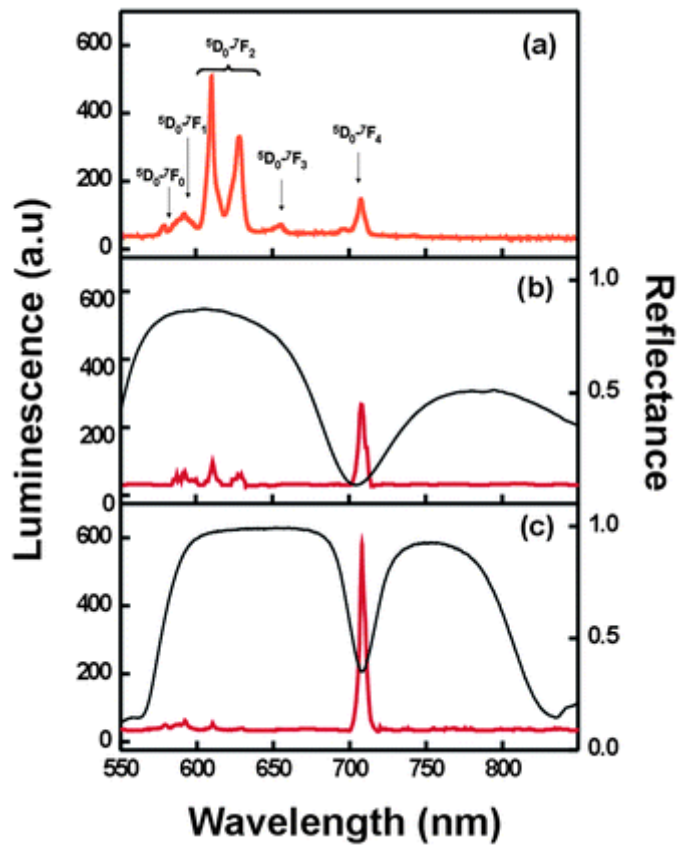


Figure 4

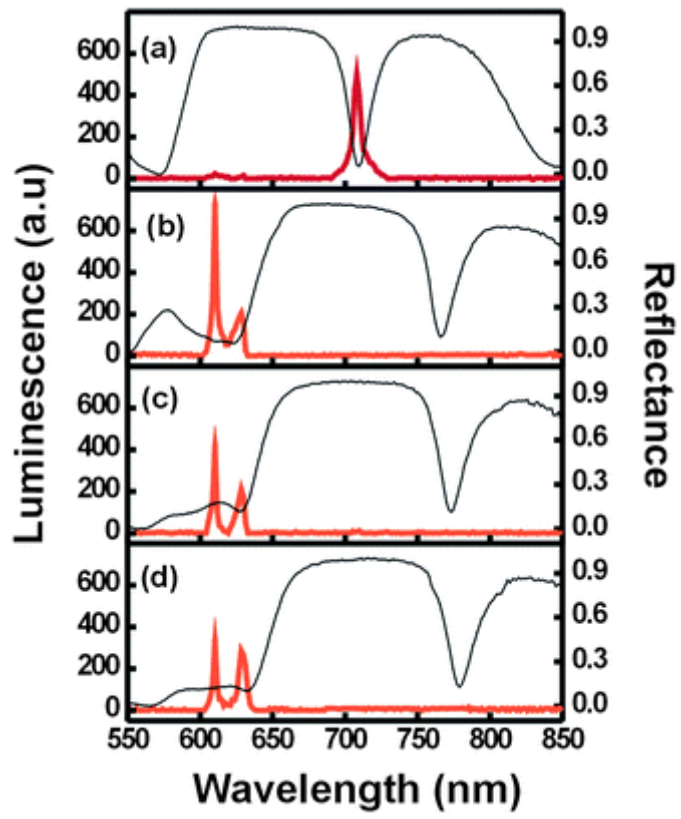


Figure 5

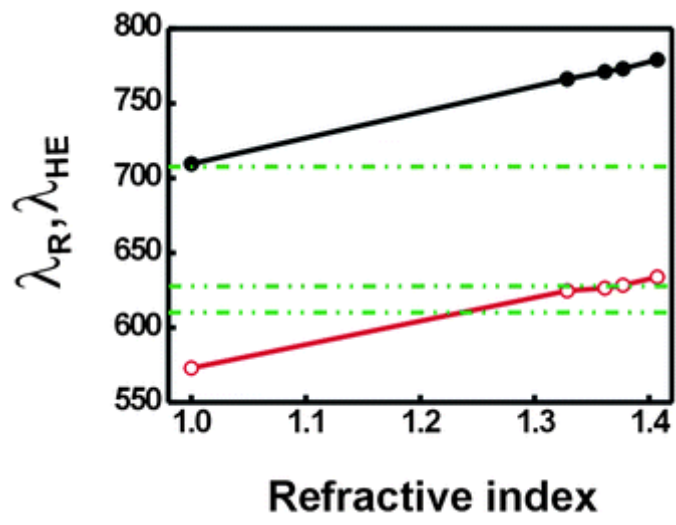


Figure 6

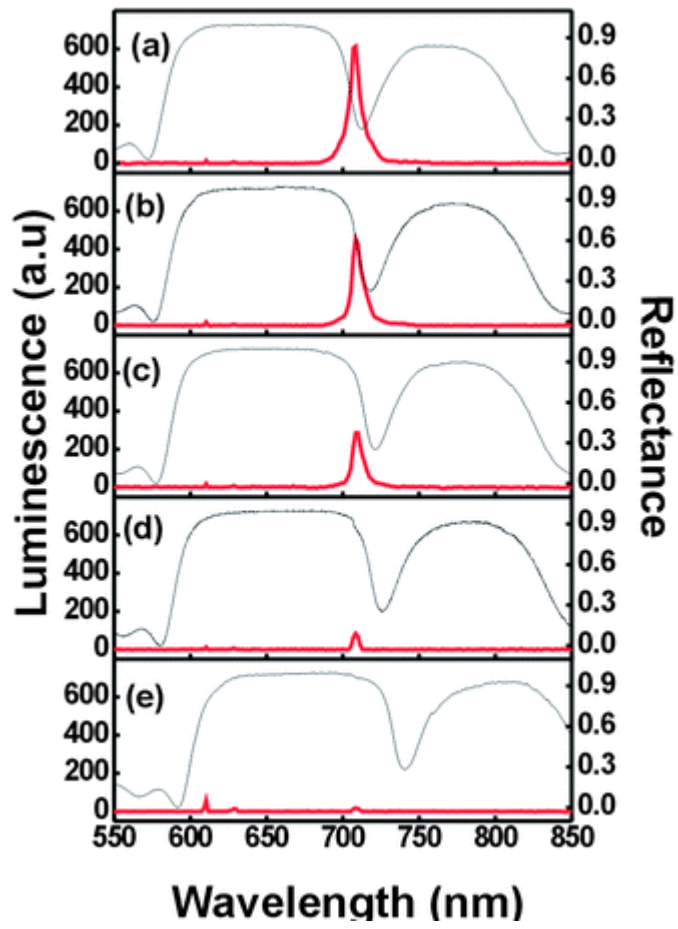


Figure 7

